

The 2015-16 El Niño

Michelle L'Heureux

Climate Prediction Center, NOAA/NWS/NCEP, College Park, Maryland

1. Evolution of the seasonal Niño SST indices during 2015-16

The El Niño of 2015-16 was among the strongest El Niño events observed since 1950, and took place almost two decades after the previous major event in 1997-98. NOAA Climate Prediction Center (CPC) issued an El Niño Advisory in March 2015. By early August 2015, seasonal Niño-3.4 sea surface temperature (SST) values were predicted by forecasters to be in excess of 2.0°C, which are values in the range of a Top 3 El Niño event.

These predictions verified as Niño 3.4 SST index were near record, peaking near 2.3°C for the average between November 2015-January 2016 (based on ERSSTv4 (Huang et al. 2015) and calculated as departures from the 1981-2010 monthly climatology; Fig. 1). The Niño-3.4 SSTs were at or in excess of +0.5°C for just over a year, between February-April (FMA) 2015 through April-June (AMJ) 2016. While the Niño-3.4 index values were impressive and competitive with the strongest El Niño events on record, two other Niño index regions clearly fell short of record setting. In particular, the easternmost Niño-3 SST and Niño-1+2 SST regions were cooler compared the 1997-98 event (Fig. 2). The latter region, near South America, also fell short of 1982-83 El Niño, and its amplitudes were more similar to the evolution of the 1972-73 event. As such, coastal Ecuador and Peru did not experience devastating rainfall and destruction as in 1982-83 and 1997-98 (personal communication, Ken Takahashi).

In contrast, the westernmost Niño-4 SST region was clearly a record when compared to three previous major El Niño events (Fig. 1). Values in this region were near or in excess of +1.0°C from early 2015 through early 2016. While impressive relative to previous events, Niño-4 SST index values were similarly elevated during the more moderate El Niño of 2009-10 (Lee and McPhaden 2010). Overall, the 2015-16 El Niño event was exceptional for its anomalous warmth in the central and east-central equatorial Pacific Ocean, while remaining relatively cooler across the eastern Pacific Ocean.

2. Global temperature, precipitation, and circulation anomalies during DJF 2015-16

During December-February (DJF) 2015-16, above-average 500-hPa geopotential heights dominated the tropical latitudes and the mid-latitudes

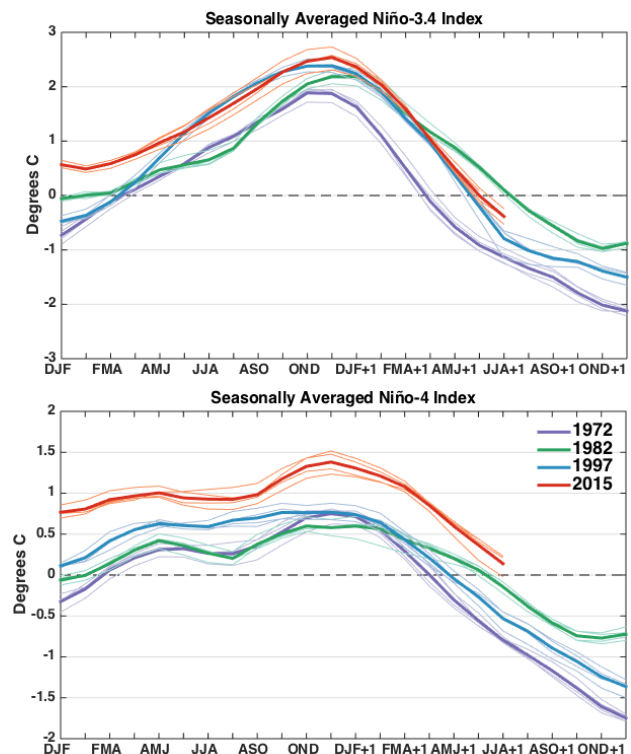


Fig. 1 Evolution of seasonal (3-month) averaged values of the Niño-3.4 SST index (top panel) and Niño-4 SST index (bottom panel) during 2015-16 (red), 1997-98 (blue), 1982-83 (green), and 1972-73 (purple). The Niño-3.4 region is 5°N-5°S, 170°-120°W and the Niño-4 region is 5°N-5°S, 150°-160°E. Thin lines correspond to the ERSSTv3b, ERSSTv4, COBE, and HadISST datasets and the thicker lines is the average of all datasets. Departures are formed by removing monthly means during 1981-2010.

of both hemispheres, with a large anticyclonic anomaly over Siberia during DJF 2015-16 (Fig. 3, top row). Associated with this pattern, strongly above-average temperatures prevailed over most of the globe, with particularly significant positive anomalies over the mid-to-high latitudes of the Northern Hemisphere (Fig. 3, middle row). The most significant regions of increased precipitation were located over the northwestern and southeastern United States, southern and eastern South America, southeast China, and just south of the equator in eastern Africa (Fig. 3, bottom row). Drier conditions were prominent over northern South America and around Indonesia.

The aspects of the circulation that were perhaps most consistent with El Niño were the distinctive wave trains tracing a great circle route across the North and South Pacific Oceans. Anomalous cyclonic flow was observed in the Gulf of Alaska and middle latitudes of the South Pacific Ocean, with anomalous anticyclones poleward and east of the anomalous troughs over Canada and closer to West Antarctica. However, the cyclonic anomaly in the Gulf of Alaska and the anticyclonic anomaly near West Antarctica were shifted northward compared to the typical El Niño response. Over North America, the anomalous warmth projected well onto the El Niño pattern, but the observed anomalies were more intense and widespread than otherwise expected with El Niño. The anticipated pattern of below-average temperatures and heights over the southern tier of the United States did not emerge. Globally, many of the regions that typically experience warmer conditions during El Niño were also above average in 2015-16, and these anomalies were more prominent.

Relative to the temperature anomalies, precipitation was more consistent with El Niño during DJF 2015-16. However, there were some notable exceptions from the El Niño pattern, such as the lack of increased precipitation over the southwestern and south-central United States. Likewise, southernmost Africa was not as dry as one might expect in an El Niño during DJF - though dry conditions over southern Africa were more prominent during ASO through OND 2015 (not shown). In northern Australia, December brought significantly more rainfall than normal, though both January and February were very much below the median, which were in line with El Niño expectations.

3. Comparison with historical global temperature and precipitation anomalies

One way to quantify the match is to compute the spatial correlation coefficient between the observed pattern and a typical El Niño pattern (global domain shown in Fig. 3). To estimate the latter, detrended DJF climate anomalies are regressed onto standardized and detrended values of the DJF Niño-3.4 index from 1979-2014. Fig. 4 shows a scatterplot of correlation coefficients between the observed pattern and the El Niño regression pattern (with the spatial mean removed) for every DJF season between 1979-2016. Overall, it shows that the larger the Niño-3.4 index value (minus or plus), the larger the strength of the pattern fit with ENSO. This figure also demonstrates that DJF 2015-16 was within the expected historical spread, though the correlations were slightly lower than the significant El Niño events of 1997-98 and 1982-83. For DJF global temperature anomalies (Fig. 4, right panel), the spatial correlation coefficient is 0.33 (10% of the observed variance is explained by the ENSO pattern), while for precipitation anomalies (Fig. 4, left panel), the spatial

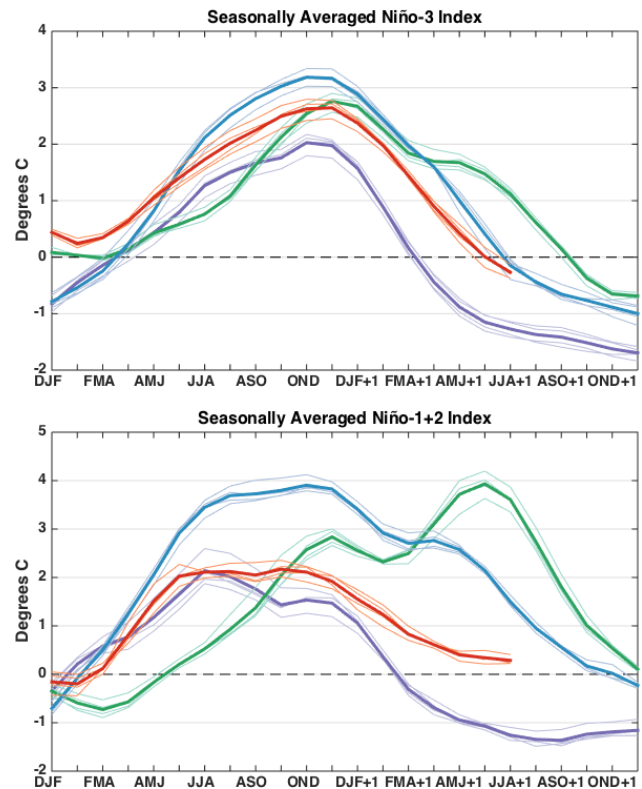


Fig. 2 Same as Figure 1, except for the Niño-3 SST index (top panel) and Niño- 1+2 SST index (bottom panel). The Niño-3 region is 5°N-5°S, 150°-90°W, and the Niño-1+2 region is 0°-10°S, 90°-80°W.

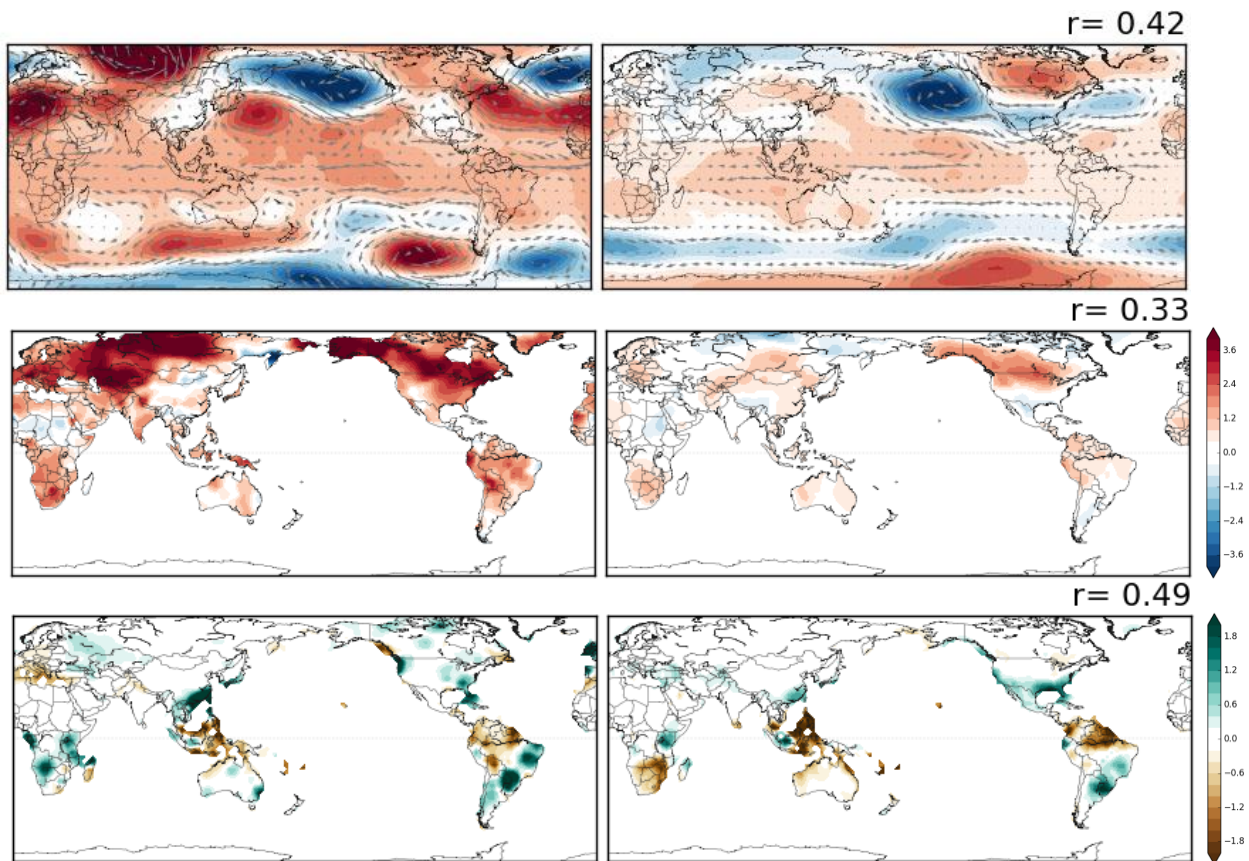


Fig. 3 December 2015-February 2016 anomalies of 500-hPa geopotential height and winds (top row), surface temperature (middle row), and precipitation (bottom row). The left column shows the observational data, while the right column shows the reconstruction for 2015/16 (weighted regression map of the Niño-3.4 index). The r -values show the spatial correlation coefficient between the observational and the reconstructed anomalies (cosine weighted by latitude). Geopotential height and wind data is from the NCEP/NCAR Reanalysis, the temperature is from the gridded GHCN+CAMS dataset (Fan and van den Dool, 2008), and precipitation data is from the gridded Precipitation Reconstruction Dataset (PREC) dataset (Chen *et al.*, 2002). Departures are formed by removing monthly means during 1981-2010.

correlation coefficient is 0.49 (24% of the variance is explained). While statistically significant, these values are not very large, and indicate that there was other variability during the Northern Hemisphere winter that was not well described by the ENSO linear regression pattern.

Acknowledgements. The NOAA/CPC ENSO forecast team: Anthony Barnston, Emily Becker, Gerry Bell, Tom Di Liberto, Jon Gottschalck, Mike Halpert, Zeng-Zhen Hu, Wanqiu Wang, Yan Xue. Portions are excerpted from the paper *Observing and Predicting the 2015-16 El Niño* online published in *Bulletin of American Meteorological Society* in 2016.

References

- Huang, B., V. F. Banzon, E. Freeman, J. Lawrimore, W. Liu, T. C. Peterson, T. M. Smith, P. W. Thorne, S. D. Woodruff, and H.-M. Zhang, 2015: Extended Reconstructed Sea Surface Temperature Version 4 (ERSST.v4). Part I: Upgrades and intercomparisons. *J. Climate*, **28**, 911–930.
- Chen, M., P. Xie, J. E. Janowiak, and P. A. Arkin, 2002: Global land precipitation: A 50-yr monthly analysis based on gauge observations. *J. Hydrometeor.*, **3**, 249–266.
- Fan, Y., and H. van den Dool, 2008: A global monthly land surface air temperature analysis for 1948-present. *J. Geophys. Res.: Atmospheres*, **113**, D01103, doi:10.1029/2007JD008470.

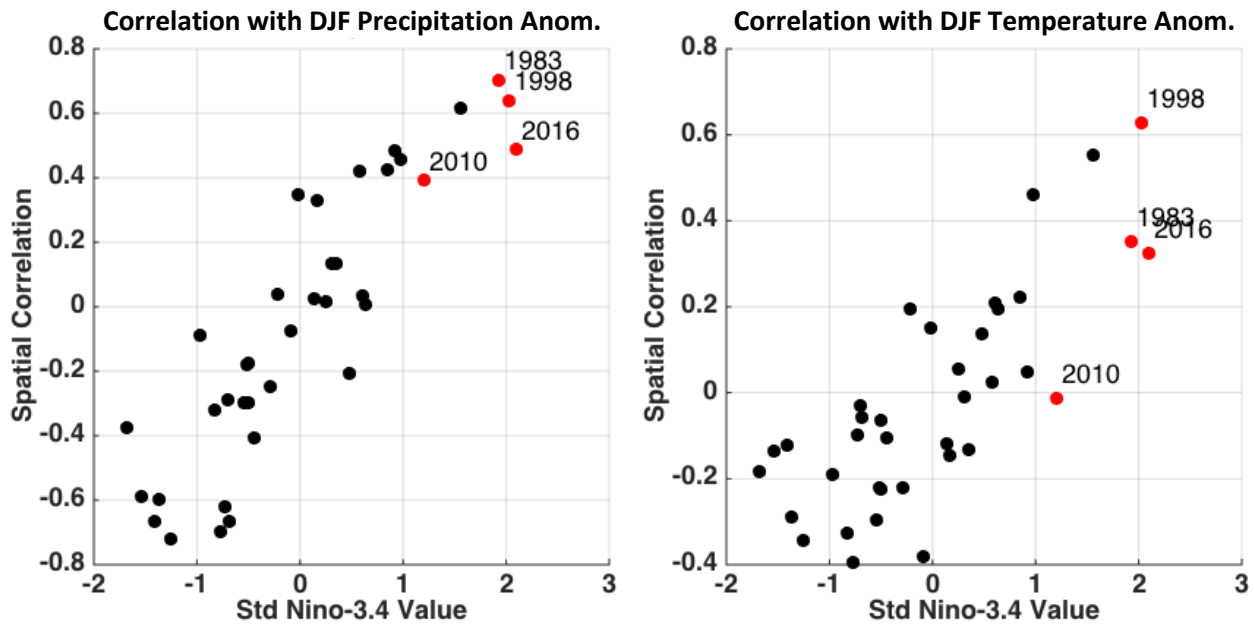


Fig. 4 The spatial correlation between the ENSO temperature (right panel) and precipitation (left panel) regression maps and observed anomalies (2015-16 shown in Figure 3). The correlation coefficient is on the ordinate and the seasonal average Nino-3.4 index value is on the abscissa. Each dot represents a single year between 1982-2016. The red dots indicate the 2015-16 El Niño, two other strong El Niños in 1997-98 and 1982-83, and the 2009-10 El Niño, which is the El Niño prior to the 2015-16 event.

L'Heureux, M., K. Takahashi, A. B. Watkins, A. G. Barnston, E. J. Becker, T. E. Di Liberto, F. Gamble, J. Gottschalck, M. S. Halpert, B. Huang, K. Mosquera-Vasquez, and A. T. Wittenberg, 2016: Observing and predicting the 2015-16 El Niño. *Bull. Amer. Meteor. Soc.*, in press, doi: 10.1175/BAMS-D-16-0009.1.

Lee, T., and M. J. McPhaden, 2010: Increasing intensity of El Niño in the central-equatorial Pacific. *Geophys. Res. Lett.*, **37**, L14603, doi:10.1029/2010GL044007.